

UC San Diego

UC San Diego Previously Published Works

Title

Chromatin Modification and Global Transcriptional Silencing in the Oocyte Mediated by the mRNA Decay Activator ZFP36L2

Permalink

<https://escholarship.org/uc/item/9bp7w5p9>

Journal

Developmental Cell, 44(3)

ISSN

1534-5807

Authors

Dumdie, Jennifer N
Cho, Kyucheol
Ramaiah, Madhuvanathi
et al.

Publication Date

2018-02-01

DOI

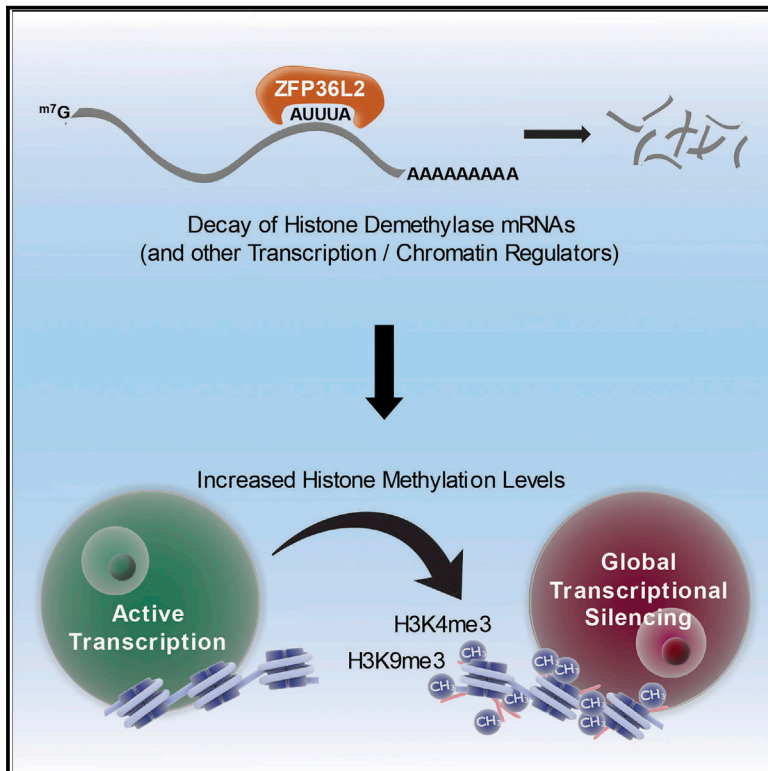
10.1016/j.devcel.2018.01.006

Peer reviewed

Developmental Cell

Chromatin Modification and Global Transcriptional Silencing in the Oocyte Mediated by the mRNA Decay Activator ZFP36L2

Graphical Abstract



Authors

Jennifer N. Dumdie, Kyucheol Cho, Madhuvanathi Ramaiah, ..., Perry J. Blackshear, Miles F. Wilkinson, Heidi Cook-Andersen

Correspondence

hcookandersen@ucsd.edu

In Brief

Global transcriptional silencing is a highly conserved developmental event central to oocyte developmental competence. Dumdie et al. report that, unexpectedly, this germline-specific global event is driven by an mRNA decay activator. ZFP36L2 downregulates master transcriptional regulators, leading to the chromatin modification and transcriptional silencing events important for oocyte competence.

Highlights

- Oocyte global transcriptional silencing is mediated by an mRNA decay activator
- ZFP36L2 downregulates master regulators of transcription during oocyte growth
- ZFP36L2 binds and degrades a group of mRNAs encoding demethylases for H3K4 and H3K9
- ZFP36L2 enables increased histone methylation associated with transcription silencing



Chromatin Modification and Global Transcriptional Silencing in the Oocyte Mediated by the mRNA Decay Activator ZFP36L2

Jennifer N. Dumdie,^{1,6} Kyuchool Cho,^{1,6} Madhuvanthy Ramaiah,^{1,6} David Skarbrevik,¹ Sergio Mora-Castilla,¹ Deborah J. Stumpo,³ Jens Lykke-Andersen,² Louise C. Laurent,¹ Perry J. Blackshear,^{3,4} Miles F. Wilkinson,^{1,5} and Heidi Cook-Andersen^{1,2,7,*}

¹Department of Reproductive Medicine, School of Medicine, University of California, San Diego, La Jolla, CA 92093, USA

²Division of Biological Sciences, University of California, San Diego, La Jolla, CA 92093, USA

³Signal Transduction Laboratory, National Institute of Environmental Health Sciences, Research Triangle Park, NC 27709, USA

⁴Departments of Medicine and Biochemistry, Duke University Medical Center, Durham, NC 27703, USA

⁵Institute of Genomic Medicine, University of California, San Diego, La Jolla, CA 92093, USA

⁶These authors contributed equally

⁷Lead Contact

*Correspondence: hcookandersen@ucsd.edu

<https://doi.org/10.1016/j.devcel.2018.01.006>

SUMMARY

Global transcriptional silencing is a highly conserved mechanism central to the oocyte-to-embryo transition. We report the unexpected discovery that global transcriptional silencing in oocytes depends on an mRNA decay activator. Oocyte-specific loss of ZFP36L2 an RNA-binding protein that promotes AU-rich element-dependent mRNA decay prevents global transcriptional silencing and causes oocyte maturation and fertilization defects, as well as complete female infertility in the mouse. Single-cell RNA sequencing revealed that ZFP36L2 downregulates mRNAs encoding transcription and chromatin modification regulators, including a large group of mRNAs for histone demethylases targeting H3K4 and H3K9, which we show are bound and degraded by ZFP36L2. Oocytes lacking *Zfp36l2* fail to accumulate histone methylation at H3K4 and H3K9, marks associated with the transcriptionally silent, developmentally competent oocyte state. Our results uncover a ZFP36L2-dependent mRNA decay mechanism that acts as a developmental switch during oocyte growth, triggering wide-spread shifts in chromatin modification and global transcription.

INTRODUCTION

The carefully orchestrated transition from the fully differentiated oocyte to the totipotent embryo is arguably one of the most dynamic transitions in biology. This oocyte-to-embryo transition fundamental to all multicellular life occurs in the absence of *de novo* transcription. Transcription is globally silenced in the final stages of oocyte growth and does not significantly resume until the two-cell embryo stage in mice. Therefore, successful devel-

opment across the oocyte-to-embryo transition requires establishment of the proper cohort of maternal mRNA and proteins within the oocyte prior to transcriptional silencing (Li et al., 2010).

Global transcriptional silencing and the acquisition of full developmental competence are closely linked events that occur during the final stages of oocyte growth. Indeed, periovulatory oocytes (referred to hereafter as GV oocytes) that fail to undergo global transcriptional silencing have significantly reduced rates of oocyte maturation, fertilization, and embryo development (Andreu-Vieyra et al., 2010; Bouniol-Baly et al., 1999; Liu and Aoki, 2002; Zuccotti et al., 2002). While some factors contributing to global transcriptional silencing have been identified (Andreu-Vieyra et al., 2010; Liu et al., 2012; Lowther and Mehlmann, 2015; Medvedev et al., 2011; Xia et al., 2012), the mechanisms underlying this pivotal developmental event remain poorly understood.

Global transcriptional silencing and developmental competence are closely associated with extensive chromatin modification, including changes in histone methylation, histone acetylation, and DNA methylation (Andreu-Vieyra et al., 2010; De La Fuente, 2006; Kageyama et al., 2007; Zuccotti et al., 2011). Among the best characterized of such modifications are increases in the levels of both histone H3K9 and H3K4 trimethylation (Dahl et al., 2016; De La Fuente, 2006; Kageyama et al., 2007; Zhang et al., 2016). H3K9me3 is widely regarded as a marker of transcriptional repression, while H3K4me3 is generally associated with active transcription (Bannister and Kouzarides, 2011). However, recent evidence provides strong support that H3K4me3 can also act as a repressive mark in oocytes and that accumulation of H3K4me3 in the late oocyte contributes to transcriptional silencing (Dahl et al., 2016; Zhang et al., 2016). The factors and pathways that mediate the accumulation of these histone methylation marks in the late oocyte and the precise functional relationships between histone methylation, transcriptional silencing, and oocyte developmental competence, remain intriguing questions.

Both transcriptional silencing and developmental competence in the oocyte are also accompanied by extensive changes in



chromatin structure. The chromatin pattern within the late mammalian oocyte nucleus shifts from a diffuse configuration (non-surrounded nucleolus [NSN]) to a condensed structure that forms a distinct ring around the nucleolus (surrounded nucleolus [SN]). *In vitro* studies have demonstrated that the SN chromatin configuration strongly correlates with transcriptional silence and full oocyte developmental competence. Conversely, the NSN chromatin configuration correlates with active transcription and significantly diminished oocyte developmental competence (Bouniol-Baly et al., 1999; Zuccotti et al., 2002). However, while transcriptional silencing and chromatin condensation are closely linked temporally, these two events are genetically separable and appear to be driven by distinct pathways (Andreu-Vieyra et al., 2010; Burns et al., 2003).

Given that the oocyte-to-embryo transition occurs in the absence of transcription, it is not surprising that this transition depends upon post-transcriptional mechanisms. Several lines of evidence suggest that RNA decay is critical for multiple stages of the oocyte-to-embryo transition (Svoboda et al., 2015), although mRNA in the growing oocyte has been proposed to be unusually stable overall (Brower et al., 1981). The mRNA decay activator ZFP36L2 has been implicated as having a role in the oocyte-to-embryo transition (Ball et al., 2014; Ramos, 2012; Ramos et al., 2004). ZFP36L2 is one of four members of the ZFP36 (TTP/Tis11) family in the mouse, all of which have established roles in degrading mRNAs harboring AU-rich elements (AREs) in the 3' UTR (Brooks and Blackshear, 2013; Sanduja et al., 2011). Each family member appears to have non-redundant, tissue-specific functions. Complete loss of ZFP36L2 in mice results in severe defects in hematopoiesis and death within a few weeks of birth (Stumpo et al., 2009). Female *Zfp36l2*-mutant mice that lack the 5' end of the *Zfp36l2* gene and express a 29 amino acid N-terminal truncated version of ZFP36L2 are infertile, with genetic background-specific blocks in ovulation or embryo development past the two-cell stage (Ball et al., 2014; Ramos et al., 2004). Because this truncated protein retains the ability to trigger mRNA decay *in vitro*, it is unclear whether the developmental arrest is a result of gain-of-function effects or reduced ARE-mediated mRNA decay activity only evident *in vivo* (Ramos, 2012). Thus, the precise role of ZFP36L2 and mRNA decay in the oocyte has remained unclear.

To establish whether ZFP36L2 plays a critical role in the oocyte and/or the oocyte-to-embryo transition, we generated and analyzed oocyte-specific *Zfp36l2* conditional knockout (cKO) mice. We found that *Zfp36l2*-cKO female mice are infertile, and oocytes from these mutant mice fail to undergo normal maturation and fertilization. To investigate the underlying mechanism, we performed single-cell RNA sequencing (RNA-seq) analysis and found that loss of ZFP36L2 caused upregulation of scores of mRNAs encoding factors with central roles in transcriptional regulation and chromatin modification, including a large group of histone demethylases that regulate methylation at H3K4 or H3K9. We show that these mRNAs are direct targets of ZFP36L2, as evidenced by mRNA decay and RNA immunoprecipitation assays, suggesting that histone methylation can be regulated by mRNA decay. Consistent with this, GV oocytes from *Zfp36l2*-cKO mice exhibited defects in H3K4 and H3K9 trimethylation and failed to undergo global transcriptional silencing, both of which are associated with the

acquisition of full developmental competence in the oocyte. Together, our findings establish an essential role for ZFP36L2 in the regulation of maternal mRNAs encoding factors that control transcription and chromatin modification and provide a mechanism by which mRNA decay can bring about histone methylation, global transcriptional silencing, and the production of a developmentally competent oocyte.

RESULTS

ZFP36L2 Expression in Oocytes Is Required for Female Fertility

To test the importance of ZFP36L2 in the oocyte-to-embryo transition, we generated cKO mice in which *Zfp36l2* is deleted only in the growing oocyte. *Zfp36l2*-floxed (*Zfp36l2*^{F/F}) mice were made harboring *loxP* sites flanking exon 2, which encodes the RNA-binding domain and the majority of the coding region (467 of 484 amino acids) (Figure S1A). Oocyte-specific deletion was achieved by crossing *Zfp36l2*^{F/F} mice (F/F or control) with mice expressing Cre recombinase driven by the *Zp3* promoter (*Zp3*-Cre), which is expressed only in growing oocytes at the primary follicle stage and onward (de Vries et al., 2000). Robust knock out in *Zfp36l2*^{F/F}; *Zp3*-Cre mice (*Zfp36l2*-cKO or cKO) was confirmed in GV oocytes at the DNA, RNA, and protein levels (Figures 1A, 1B, S1A, and S1B). Adult *Zfp36l2*-cKO females displayed normal estrus cycles (Figure S1C) and mating behavior (Figure S1D). However, crosses with wild-type males revealed that *Zfp36l2*-cKO females were completely infertile (Figure 1C), demonstrating that oocyte-specific expression of ZFP36L2 is required for female fertility.

ZFP36L2 Is Required for Oocyte Developmental Competence

Histological analyses of ovaries from cKO and control adult females were performed to investigate whether ZFP36L2 has roles in oocyte and/or follicle growth. These studies revealed that ovaries of cKO females contained follicles at all developmental stages (Figure 1D). Quantification of whole ovaries from unstimulated adult cKO and control females showed overall similar numbers of follicles at each stage of growth and similar numbers of corpora lutea (Figure 1E), demonstrating that oocyte-specific expression of ZFP36L2 is not required for growth to the GV stage or for ovulation. Further, GV stage oocytes isolated from cKO and control females were indistinguishable from controls with respect to oocyte morphology and diameter (Figure S1E). However, follicle counts in cKO ovaries did demonstrate lower numbers of primary follicles and a trend toward lower numbers of follicles at later stages (Figure 1E). To examine this potential defect more closely, we repeated the quantification of follicles in ovaries from sexually immature females following pharmacological ovarian stimulation. Following gonadotropin challenge, cKO ovaries contained fewer growing follicles and corpora lutea relative to control ovaries (Figure S1F). cKO ovaries also had higher numbers of atretic oocytes compared with control ovaries, specifically at the primary and secondary stages (Figures S1F and S1G). Together, these findings suggest a role for ZFP36L2 in the early preantral follicle. However, that similar numbers of oocytes grew to the GV stage and were ovulated in adult cycling mice demonstrates that the

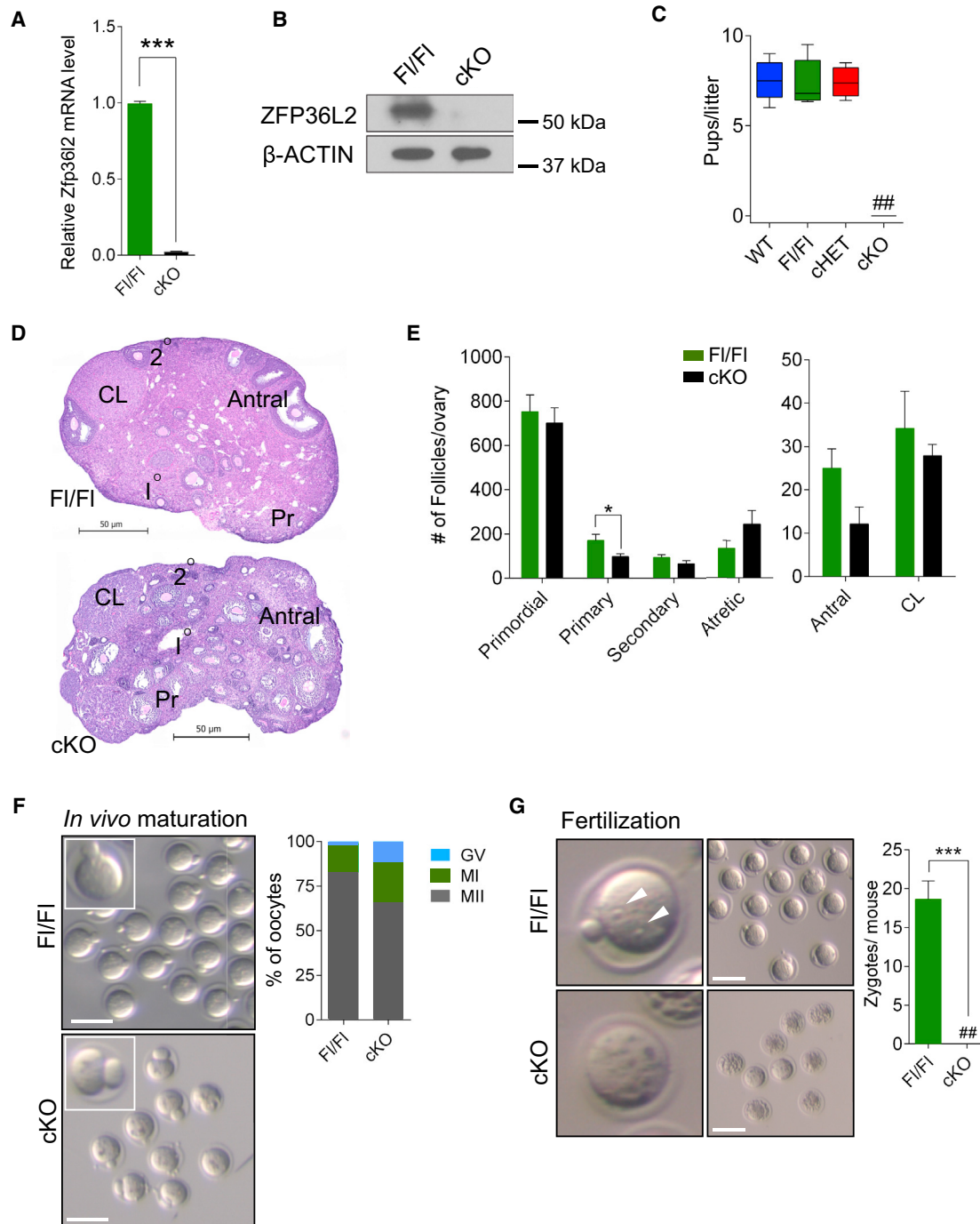


Figure 1. ZFP36L2 Expression in Oocytes Is Required for Female Fertility and Oocyte Developmental Competence

(A) Relative level of *Zfp36l2* mRNA by qPCR analysis in cKO and F1/F1 GV oocytes, normalized to *Gapdh*. Error bars are SEM (unpaired t test; *** $p < 0.001$).

(B) Western blot comparing ZFP36L2 in cKO and F1/F1 GV oocytes. β -Actin is the internal loading control.

(C) Boxplot showing the distribution of the number of pups/litter for cKO and controls over a 6-month period. ##, no pups.

(D) H&E stained sections of ovaries from unstimulated adult F1/F1 and cKO females. Pr, primordial; 1 $^{\circ}$, primary; 2 $^{\circ}$, secondary; CL, corpus luteum. Scale bar, 50 μ m.

(E) Number of follicles at each stage of development in whole ovaries of mature unstimulated F1/F1 and cKO mice. Bars represent mean and error bars show SEM at each stage of development (unpaired t test; * $p < 0.05$).

(F) Number of GV, MI, and MII oocytes isolated from cKO and F1/F1 females following superovulation *in vivo* as a percent of total oocytes. Insets, MII oocyte enlarged to show the abnormally large polar bodies observed in many cKO oocytes. Scale bar, 100 μ m.

(G) Number of zygotes isolated from cKO and F1/F1 females following superovulation and mating. Bars represent mean values and error bars show SEM (unpaired t test; *** $p < 0.001$; ##, no zygotes). Arrowheads in top left panel indicate pronuclei identified only in F1/F1. Scale bar, 100 μ m.

See also [Figures S1](#) and [S2](#).

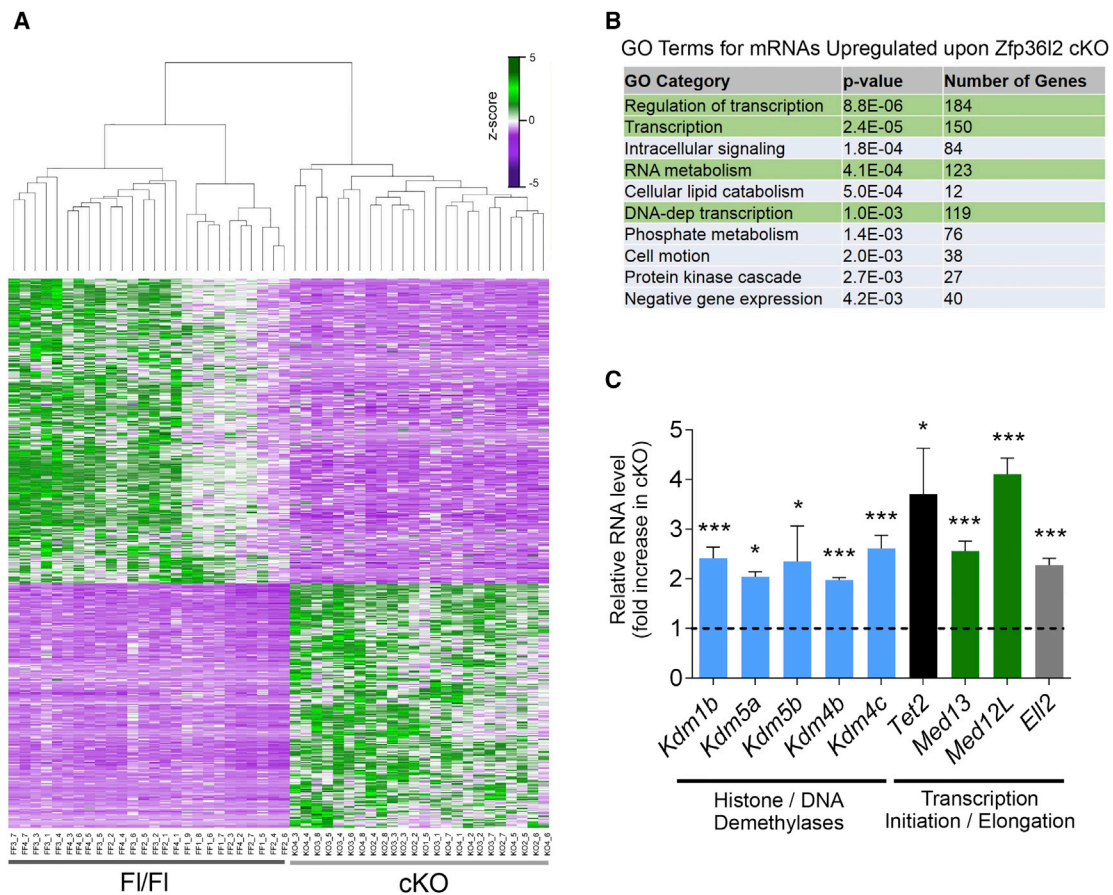


Figure 2. ZFP36L2 Regulates mRNAs Encoding Factors with Central Roles in Transcription Regulation and Chromatin Modification

(A) Heatmap depicting clustering and global changes in gene expression for GV oocytes from FI/FI and cKO females as determined by single-cell RNA-seq. (B) GO analysis of transcripts upregulated in cKO oocytes show enrichment for genes involved in transcription regulation (green). Top ten most highly enriched categories are shown. (C) qPCR validation for a subset of changes observed in FI/FI and cKO oocytes by RNA-seq. RNA levels are shown relative to *L19* and FI/FI oocytes were normalized to 1; error bars are SEM (unpaired t test; * $p < 0.05$; *** $p < 0.001$).

complete infertility of adult cKO females cannot be explained by a gross defect in oocyte growth, folliculogenesis, or ovulation alone.

To uncover the cause of female infertility in the *Zfp36l2*-cKO mice, we next investigated the role of ZFP36L2 in oocyte maturation and fertilization. Consistent with our histological analyses above, cKO females failed to upregulate oocyte production following gonadotropin stimulation (4 ± 3.6 versus 23 ± 7.7 ovulated in cKO and FI/FI, respectively). In further analyses, cKO oocytes exhibited significantly lower rates of maturation than control oocytes, both following superovulation *in vivo* (63% in cKO versus 85% in control, $p = 0.025$) (Figure 1F) and following culture of cumulus-oocyte complexes *in vitro* (51% in cKO versus 76% in control, $p = 0.04$) (Figure S1H). Many of the cKO oocytes that reached the MII stage displayed abnormally large polar bodies, a phenotype suggestive of a spindle defect (Figures 1F and S1H, insets). Following superovulation and mating experiments to examine fertilization, no zygotes were recovered from 8 cKO females compared with 95 zygotes from 5 control females, demonstrating that cKO oocytes are incompetent to undergo fertilization (Figure 1G). Together, these re-

sults demonstrate that oocytes lacking *Zfp36l2* exhibit abnormal oocyte maturation and a failure to undergo normal fertilization, establishing a critical role for oocyte-specific expression of ZFP36L2 in oocyte developmental competence and female fertility.

ZFP36L2 Regulates mRNAs Encoding Factors with Central Roles in Transcription Regulation and Chromatin Modification

Given the well-established role of ZFP36L2 in mRNA degradation, we next sought to identify oocyte mRNAs dysregulated as a consequence of *Zfp36l2*-cKO. To this end, we performed single-cell RNA-seq analyses, comparing GV oocytes from 26 control and 24 cKO females. cKO oocytes exhibited gene expression patterns distinct from control oocytes, as shown by both hierarchical clustering (Figure 2A) and unbiased principal component analysis (Figure S2A). Analysis of control RNAs covering a wide range of known lengths and concentrations spiked in to the single-cell RNA-seq reactions (Baker et al., 2005; External RNA Controls Consortium, 2005) showed read counts correlated with input concentrations (Figure S2B) and

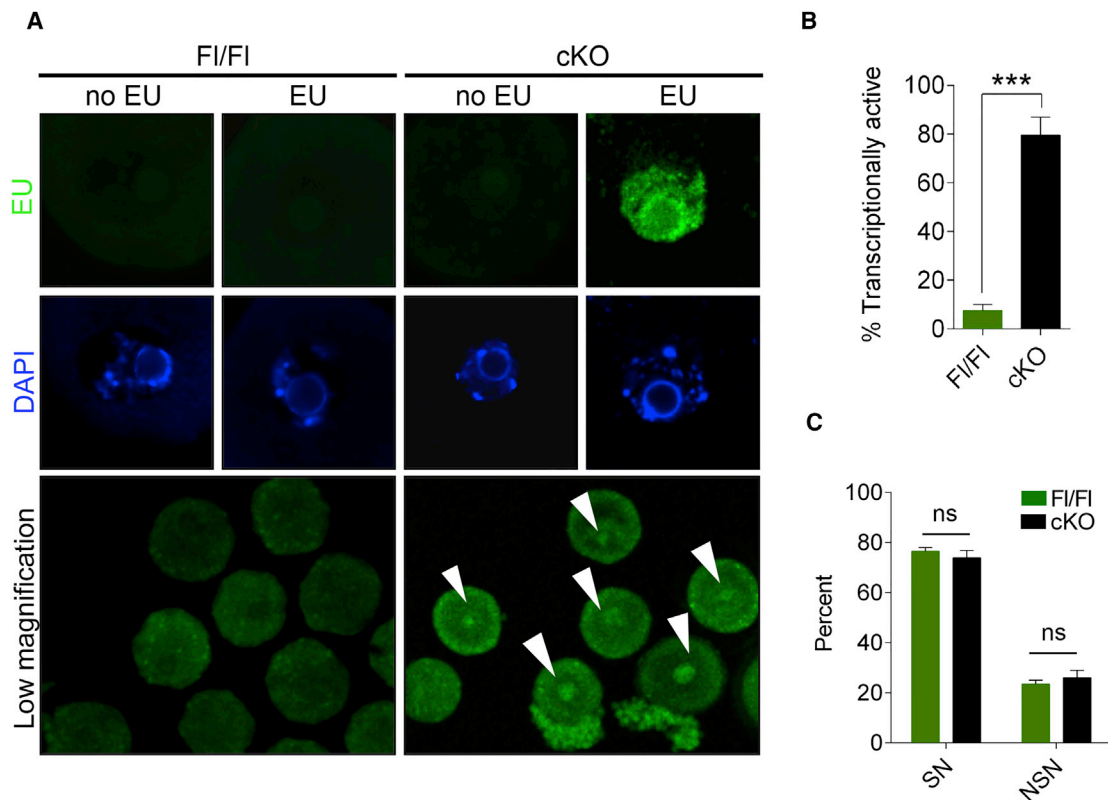


Figure 3. ZFP36L2 Is Required for Global Transcriptional Silencing during the Final Stages of Oocyte Growth

(A) Run-on transcription assays performed in cKO and F1/F1 GV oocytes by culture in the presence or absence of 5-ethynyl uridine (EU). Newly transcribed, EU-labeled cellular RNAs are detected as green fluorescence following staining; nuclei are blue (Hoechst). A lower-magnification image demonstrates the range of transcriptional activity observed; arrowheads indicate transcriptionally active nuclei to the extent visible in a single confocal plane.

(B) The percent of transcriptionally active oocytes in run-on assays from (A) is quantified. Error bars are SEM (unpaired t test; *** $p < 0.001$).

(C) Chromatin organization of oocytes in the run-on assays was determined by Hoechst staining. Error bars are SEM (unpaired t test; ns, nonsignificant).

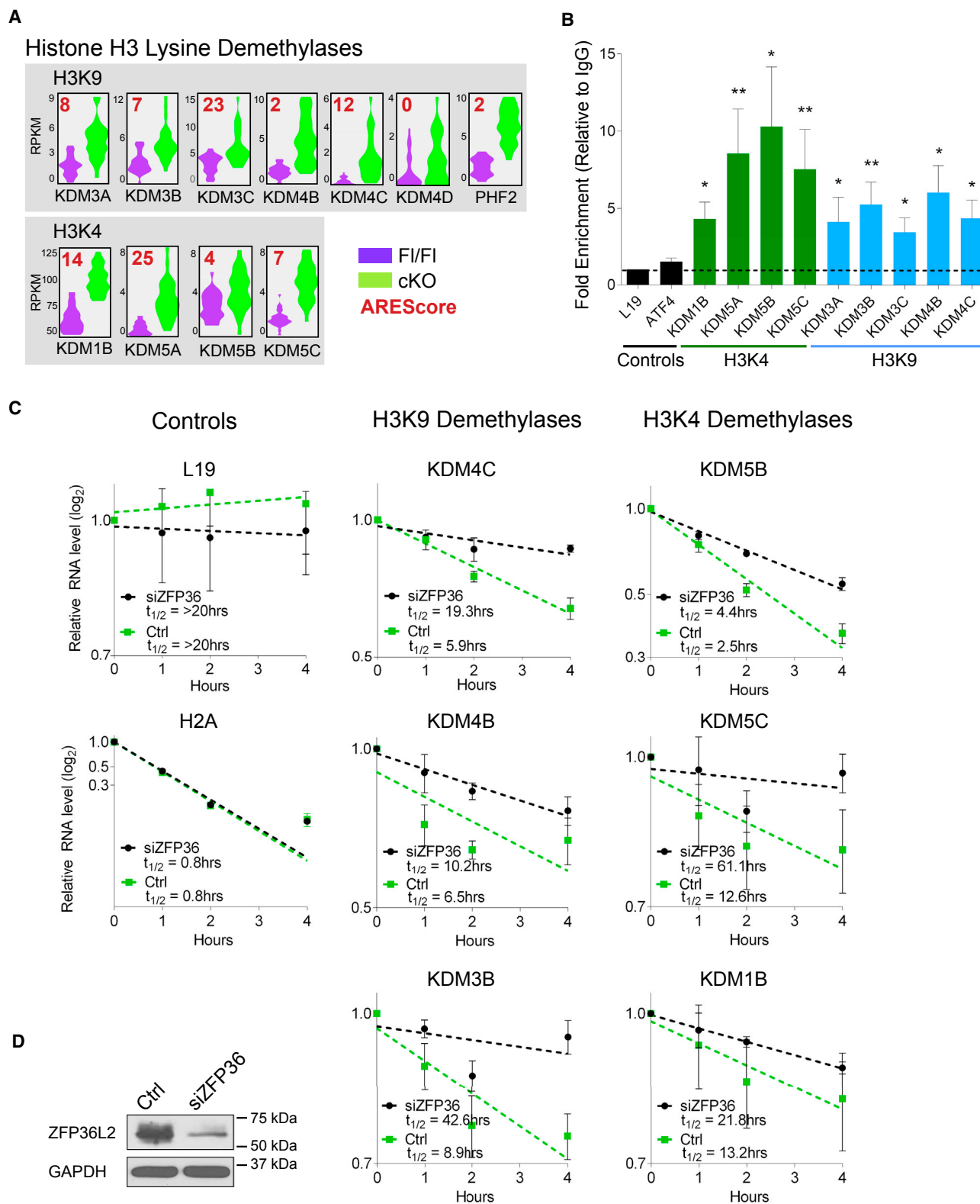
no significant differences in overall read counts in cKO versus control oocytes (Figure S2C). These data provide a robust validation of our RNA-seq pipeline and demonstrate that *Zfp36l2* cKO does not result in a large, nonspecific shift for a substantial fraction of the polyadenylated mRNA pool in the oocyte. Instead, our transcriptome analyses revealed significant, reproducible changes in the levels of a subset of mRNAs in the absence of ZFP36L2 (Figure 2A; Table S1). Of 16,614 mRNAs with detectable expression in single oocytes, we observed higher levels of 1,418 (8.5%) and lower levels of 1,201 (7.2%) transcripts in cKO oocytes relative to controls (\log_2 fold change > 1 ; adjusted p value (Q) < 0.05), consistent with a significant role for ZFP36L2 in regulating the mRNA pool during oocyte growth.

Because ZFP36L2 is known to trigger mRNA decay, mRNAs upregulated by *Zfp36l2* deletion are candidates to be direct targets of ZFP36L2. Consistent with this, transcripts upregulated upon *Zfp36l2*-cKO were enriched for mRNAs that associate with ZFP36L2 in mouse erythroid cells (Zhang et al., 2013) (Figure S2E). Moreover, transcripts that were both upregulated in *Zfp36l2*-cKO oocytes and bound by ZFP36L2 in mouse erythroid cells were enriched for 3' UTR AREs, relative to downregulated and unbound mRNAs, as measured by higher AREScores (Figure S2F), a metric shown to correlate with mRNA decay triggered by ZFP36 proteins (Spasic et al., 2012). Gene ontology

(GO) analysis revealed that the two most highly enriched categories among mRNAs upregulated with *Zfp36l2* deletion were *Regulation of Transcription* ($p = 8.8 \times 10^{-6}$; 184 genes) and *Transcription* ($p = 2.4 \times 10^{-5}$; 150 genes) (Figure 2B). In all, four of the top six most highly enriched categories related to transcription regulation and chromatin modification. We validated a subset of upregulated mRNAs encoding transcription regulators with low, medium, and high fold changes by qRT-PCR (Figure 2C). GO analysis of mRNAs downregulated in cKO oocytes, which would be expected to be regulated indirectly by ZFP36L2, encoded proteins enriched for several biological pathways not obviously relevant to oocyte development (Figure S2D).

ZFP36L2 Is Required for Global Transcriptional Silencing during the Final Stages of Oocyte Growth

Our discovery that oocytes lacking ZFP36L2 exhibit dysregulated expression of many transcriptional regulators raised the possibility that ZFP36L2 is important for oocyte transcriptional silencing. To directly test this, we performed transcriptional run-on assays using 5-ethynyl uridine, followed by fluorescence staining, to examine transcription activity on a global scale. Strikingly, we found that $\sim 80\%$ of GV oocytes from cKO mice failed to undergo transcriptional silencing (Figures 3A and 3B). In contrast, only 8% of control GV oocytes had this phenotype.



(legend continued on next page)

This transcriptional silencing defect occurred in the absence of a gross defect in chromatin organization, with a similar number of cKO oocytes reaching the SN configuration (74% cKO versus 76% FI/FI) (Figure 3C). These observations demonstrate an essential role for the mRNA decay activator, ZFP36L2, in mediating global transcriptional silencing independent of chromatin condensation in the late oocyte.

mRNAs Encoding Histone Demethylases for H3K4 and H3K9 Are Direct Targets of ZFP36L2 Decay

To identify mRNAs that ZFP36L2 might regulate to drive global transcriptional silencing, we evaluated the effect of *Zfp36l2*-cKO on groups of mRNAs in more than 1,400 narrow GO categories. This identified *Histone demethylases* as a group that was significantly upregulated upon *Zfp36l2*-cKO (Figure S3A). We next investigated whether these are ZFP36L2 direct targets. Such direct target mRNAs would be expected to not only be upregulated in oocytes with *Zfp36l2*-cKO, but to also (1) contain 3' UTR AREs, (2) be bound by ZFP36L2, and (3) be stabilized in the absence of ZFP36L2. In support, we found that histone demethylase mRNAs demonstrated AU-rich 3' UTRs with high AREScores compared with mRNAs for other transcription regulators (Figure S3B). This group of histone demethylase mRNAs was also enriched for binding to ZFP36L2 in mouse erythroid cells (Figure S3C), relative to groups of mRNAs encoding other chromatin modifiers and to all other expressed transcripts as a whole.

Remarkably, 11 of the 12 histone demethylase mRNAs that were upregulated in the absence of ZFP36L2 encode demethylases for histone H3K4 or H3K9 (Figure 4A). Examination of individual transcripts revealed the majority of these mRNAs (8 of 11) contain AU-rich 3' UTRs with AREScores of ≥ 4 , predictive of ARE-mediated mRNA decay (Spasic et al., 2012) (Figure 4A). In support of the functional importance of these AU-rich 3' UTR sequences, a high AREScore is an evolutionary conserved feature of this group of histone demethylase mRNAs in mammals (Figure S3D). In contrast, we only identified two histone demethylase mRNAs that were modestly downregulated (1.5–1.7-fold) (Table S1).

To test whether histone demethylase mRNAs are bound and degraded by ZFP36L2, we turned to HeLa cells, where ZFP36L2 is the predominant ZFP36-family protein expressed (Nagaraj et al., 2011; Paulo and Gygi, 2017), and assessment of its mRNA association and degradation activity was feasible. RNA-immunoprecipitation analysis using an antibody specific for ZFP36L2 revealed that ZFP36L2 associated with each of the histone H3K4 and H3K9 demethylase mRNAs upregulated in the absence of ZFP36L2 in the oocyte (Figure 4B). Depletion of ZFP36L2 using a validated small interfering RNA targeting human ZFP36 proteins (Jing et al., 2005) resulted in stabilization of the majority of these histone demethylase mRNAs (Figures 4C,

4D, and S3E). Together, these findings provide strong evidence that H3K4 and H3K9 histone demethylase mRNAs are direct targets of ZFP36L2-mediated RNA decay.

ZFP36L2 Mediates Global Increases in H3K4 and H3K9 Methylation in the Final Stages of Oocyte Growth

Our findings raised the question of whether ZFP36L2 acts to downregulate histone demethylase mRNAs to drive increased methylation levels at H3K4 and H3K9, changes closely associated with transcriptional silencing and chromatin condensation in competent oocytes (De La Fuente, 2006; Kageyama et al., 2007). Immunofluorescence analyses performed in cKO and control GV oocytes to investigate this possibility revealed marked differences in the nuclei of cKO relative to control oocytes. Despite the ability of *Zfp36l2*-cKO oocytes to successfully complete the transition from the NSN to SN chromatin configuration (Figures 3A, 3C, 5A, and S4), oocytes lacking ZFP36L2 failed to upregulate both histone H3K4 and H3K9 trimethylation, while overall levels of histone H3 were not significantly affected (Figures 5A, 5B, and S4). This defect was specific for SN oocytes, as levels of H3K4me3 and H3K9me3 were low in NSN oocytes both in the presence and absence of ZFP36L2. To confirm, we performed western blot analyses, which verified significantly lower levels of H3K4me3 in *Zfp36l2*-cKO relative to control oocytes (Figure 5C). We also attempted western blot analysis with multiple antibodies against H3K9me3, but were unable to detect a signal with a feasible number of oocytes. Together, these data indicate a critical role for ZFP36L2 in the accumulation of both H3K4 and H3K9 trimethylation that occurs in the final stages of growth in the transcriptionally silent, fully competent oocyte.

DISCUSSION

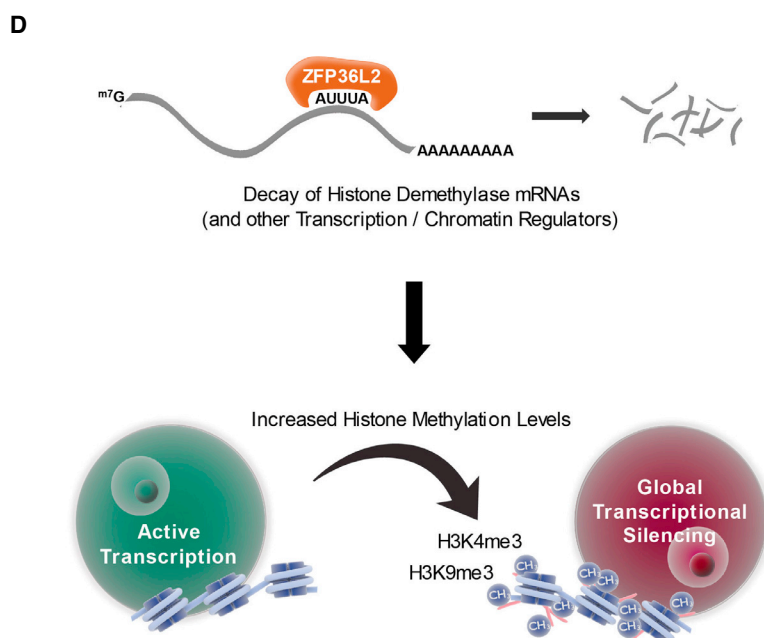
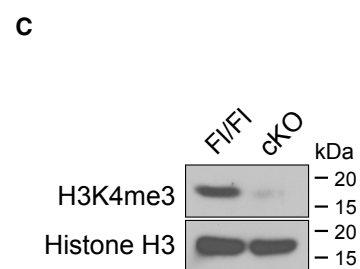
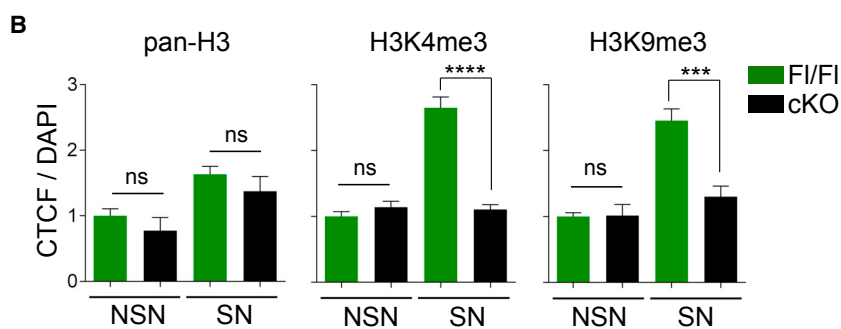
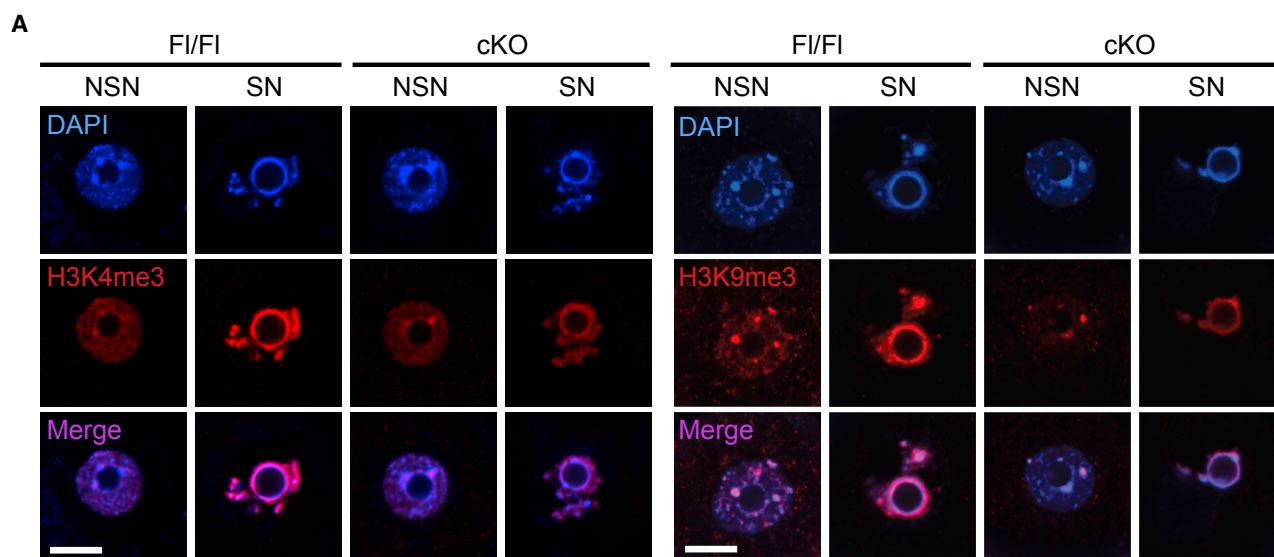
Global transcriptional silencing is a highly conserved event in the final stages of oocyte growth tightly linked to the successful transition from oocyte to embryo (Andreu-Vieyra et al., 2010; Liu and Aoki, 2002; Zuccotti et al., 2002). Our study reveals a critical role for an mRNA decay factor, ZFP36L2, in regulating histone modification and bringing about this transcriptional silencing event (Figure 5D).

Our findings suggest that the role of ZFP36L2 in global transcriptional silencing in the oocyte occurs, at least in part, through a direct effect of ZFP36L2 on mRNA stability during oocyte growth. Our single-cell transcriptome analyses identified a group of mRNAs encoding histone H3K4 and H3K9 demethylases that are upregulated in the oocyte with *Zfp36l2*-cKO (Figures 2C, 4A, and S3A), contain 3' UTR AREs conserved among mammals (Figures 4A, S3B, and S3D), are bound by ZFP36L2 in both human HeLa cells (Figure 4B) and mouse erythroid cells (Figure S3C) (Zhang et al., 2013), and, for the majority, are stabilized

(B) RNA immunoprecipitation assay demonstrating fold enrichment for ZFP36L2 binding for each histone demethylase mRNA in HeLa cells relative to immunoglobulin G (IgG) control and normalized to L19. ATF4 is an additional control mRNA subjected to an mRNA decay pathway not dependent on ZFP36L2. Bars represent mean values and error bars show SEM (two-way ANOVA; * $p < 0.05$; ** $p < 0.01$).

(C) RNA decay assay showing increased half-lives for histone demethylase mRNAs as determined by qPCR in HeLa cells following knock down of ZFP36L2. Cells were transfected with small interfering RNA (siRNA) targeting either ZFP36 proteins or luciferase as a control, then treated with actinomycin D for the indicated times. Points represent mean RNA levels relative to $t = 0$ normalized to GAPDH levels as a stable internal control. Error bars represent SEM. Half-life was not determined for L19 as the regression line was near horizontal. See Figure S3E for additional mRNAs evaluated.

(D) Western blot for ZFP36L2 demonstrating knock down following siRNA transfection in HeLa cells. GAPDH is the internal loading control.



(legend on next page)

upon ZFP36L2 depletion (Figures 4C, 4D, and S3E). Collectively, these findings strongly suggest that these histone demethylase mRNAs are direct targets of ARE-mediated decay by ZFP36L2 in the oocyte. Functional importance of downregulation of this group of H3K4 and H3K9 demethylase mRNAs by ZFP36L2 in the oocyte is suggested by our finding that loss of *Zfp36l2* resulted in a failure to accumulate increased levels of histone H3K4me3 and H3K9me3 (Figures 5A–5C), marks with demonstrated roles in transcriptional repression (Bannister and Kouzarides, 2011; Dahl et al., 2016; Zhang et al., 2016) and closely associated with both global transcriptional silencing and the developmentally competent oocyte state. In contrast, chromatin condensation (another important developmental event in the late oocyte) occurred independently of ZFP36L2 (Figures 3A, 3C, 5A, and S4). Together, our findings suggest a mechanism whereby ZFP36L2 acts as a developmental switch in the oocyte to downregulate a group of histone demethylase mRNAs to drive increased H3K4 and H3K9 methylation levels, global transcriptional silencing, and the production of a developmentally competent oocyte (Figure 5D).

An important issue for the future is determining the precise role of ZFP36L2-dependent histone H3K4 and H3K9 methylation in regulating chromatin structure and transcriptional silencing in the oocyte. While histone methylation has been implicated in the regulation of higher-order chromatin structure (Bannister and Kouzarides, 2011), our results demonstrate wild-type oocyte levels of these histone marks are not necessary for (or induced by) chromatin condensation from the NSN-to-SN configuration (Figures 3A, 3C, 5A, and 5B). H3K9me3 is a strong candidate for a transcriptional repressive mark, as it is associated with transcriptional repression in a wide variety of cell types (Bannister and Kouzarides, 2011), and we and others observed increases in H3K9me3 levels concomitant with global transcriptional silencing in oocytes (Figures 5A and 5B) (De La Fuente, 2006; Kageyama et al., 2007). In contrast, while H3K4me3 is widely considered to be a mark of active transcription in somatic cells (Bannister and Kouzarides, 2011), several lines of evidence suggest that this mark can play the opposite role in the oocyte. H3K4me3 levels are higher in transcriptionally silent SN oocytes relative to transcriptionally active NSN oocytes (Figures 5A and 5B) (De La Fuente, 2006; Kageyama et al., 2007). Moreover, knock out of the H3K4 methyltransferase, MLL2, leads to lower levels of H3K4me3 in the face of persistent transcriptional activity (Andreu-Vieyra et al., 2010). Finally, it was recently shown that removal of H3K4me3 in transcriptionally silent oocytes by forced overexpression of KDM5B, one of the histone demethylases we observed upregulated in *Zfp36l2*-cKO oocytes and regulated by ZFP36L2, partially restores transcriptional activity

(Figures 2C and 4A–4C) (Zhang et al., 2016). Together, these observations strongly implicate both H3K9 and H3K4 methylation as marks involved in transcriptional repression in oocytes. Of note, we observed no significant effect on *Mll2* mRNA levels in *Zfp36l2*-cKO oocytes, and, in contrast to histone demethylases, histone methyltransferases as a group did not stand out as potential ZFP36L2 targets (Figures S3A–S3C; Table S1). This suggests that ZFP36L2 affects the balance of histone H3K4 and H3K9 methylation by targeting histone demethylases rather than histone methyltransferases and implicate mRNA decay as an important mechanism contributing to the epigenetic changes established in the late oocyte in preparation for the oocyte-to-embryo transition.

How is ZFP36L2-mediated mRNA decay regulated to allow timely transcriptional silencing? It is well established that ZFP36 family members are regulated post-translationally by phosphorylation, with each member containing upward of ten phosphorylation sites, more than one of which have been shown to regulate mRNA decay-promoting activity (Sanduja et al., 2011). Therefore, while ZFP36 proteins are expressed in a wide range of cell types and tissues, their mRNA decay-promoting activity is likely to be dynamically regulated, and the specific pathways regulating ZFP36L2 decay activity in the oocyte are not known. In addition, we note that our single-cell RNA-seq analyses did not detect deadenylated mRNA, and our studies are not able to distinguish between deadenylated and degraded mRNAs. Thus, determining whether histone demethylase and/or other mRNAs targeted by ZFP36L2 in the oocyte are degraded or accumulate as deadenylated transcripts for later decay or reactivation by polyadenylation is an interesting future question.

In addition to the role for oocyte expression of ZFP36L2 in global transcriptional silencing during oocyte growth shown here, ZFP36L2 and the ARE-mediated mRNA decay pathway likely play important roles at other stages of oocyte and early embryo growth as well. While oocytes lacking ZFP36L2 were able to grow and ovulate at relatively normal rates in unstimulated adult females (Figures 1D, 1E, and S1E), stimulation of sexually immature and peri-pubertal cKO females with exogenous gonadotropin uncovered a likely additional role for ZFP36L2 in early preantral follicle growth (Figures S1F and S1G). Such a role could be in early oocyte growth or survival or in communication of the oocyte with the surrounding follicular cells, given the observed decrease in response to gonadotropin stimulation. It is also possible that decay of other ZFP36L2 mRNA targets not investigated here contribute to the defects in global transcriptional silencing, oocyte maturation, and fertilization observed in *Zfp36l2*-cKO females. Roles for

Figure 5. ZFP36L2 Mediates Global Increases in H3K4 and H3K9 Methylation in the Final Stages of Oocyte Growth

(A) Immunofluorescence of cKO and F1/F1 GV oocytes with SN and NSN chromatin configurations to compare H3K4me3 and H3K9me3 levels. See also Figure S4A for pan-H3 analyses. Scale bar, 10 μ m.

(B) Quantification of immunofluorescence intensity as seen in (A) and Figure S4A. Corrected total cell fluorescence (CTCF) was calculated for each signal then normalized to DAPI CTCF and to the respective F1/F1 NSN intensity, which was set to 1. Bars represent mean values and error bars show SEM (unpaired t test; ***p < 0.001; ****p < 0.0001).

(C) Western blot comparing H3K4me3 levels in cKO and F1/F1 oocytes. Total histone H3 levels serve as internal loading control.

(D) Model for the role of the mRNA decay activator ZFP36L2 in the oocyte. We propose that ZFP36L2 acts as a developmental switch during oocyte growth by binding and directly degrading a group of mRNAs encoding H3K4 and H3K9 histone demethylases, leading to the accumulation of histone methylation at H3K4 and H3K9, global transcriptional silencing, and the acquisition of full developmental competence.

ZFP36L2 in oocyte maturation and embryo development past the two-cell stage are evident from published studies with mice globally expressing a short N-terminal truncated version of ZFP36L2, although it is not known whether these roles represent a requirement for ZFP36L2 activity in the oocyte, the embryo, or another cell type (Ball et al., 2014; Ramos et al., 2004). However, given that significant decay of maternal mRNA is known to occur during both oocyte maturation and the two-cell embryo stage before the maternal-zygotic transition, it is tempting to speculate that ZFP36L2 is involved in decay at one or both of these stages.

There is a growing consensus that regulation of mRNA degradation during development might act as a developmental switch a powerful means to switch from one program to another at pivotal developmental transitions (Svoboda et al., 2015). Our findings demonstrate such a role for an mRNA degradation pathway in establishing transcriptional silence and developmental competence in the final stages of oocyte growth. In particular, our demonstration that a post-transcriptional pathway controls the levels of multiple histone demethylase mRNAs is an unexpected finding that opens exciting avenues of investigation into the role of mRNA decay in regulating chromatin modification. The potential impact of these findings is strengthened given our data suggesting that ARE-mediated decay of this group of mRNAs is a conserved process. Conservation of this pathway also raises the interesting possibility that defects in ZFP36L2 activity might play a role in a subset of currently unexplained causes of human female infertility. Together, that transcriptional silencing on a global scale is mediated by an mRNA decay activator acting on key regulators of transcriptional activity is an exciting possibility with broad implications for both development and transcriptional regulation. These data provide a compelling demonstration of the importance of mRNA decay at a pivotal developmental transition.

STAR★METHODS

Detailed methods are provided in the online version of this paper and include the following:

- **KEY RESOURCES TABLE**
- **CONTACT FOR REAGENT AND RESOURCE SHARING**
- **EXPERIMENTAL MODEL AND SUBJECT DETAILS**
 - Generation of Conditional Knockout Mice
 - Primary Culture of Oocytes and Zygotes
 - Maintenance of Cell Lines
- **METHOD DETAILS**
 - Genotyping and DNA PCR
 - Fertility and Estrus Cycle Assessment
 - Ovarian Follicle Counts
 - Evaluation of Oocyte Diameter
 - Ovulation, Maturation and Fertilization
 - Single Cell Library Preparation
 - RNA Sequencing and Data Analysis
 - RNA Isolation and qPCR Analysis
 - Run-on Transcription Assays
 - Western Blotting
 - Immunofluorescence
 - RNA Immunoprecipitation

- RNA Decay Assays
- ARE Conservation
- **QUANTIFICATION AND STATISTICAL ANALYSIS**
- **DATA AND SOFTWARE AVAILABILITY**

SUPPLEMENTAL INFORMATION

Supplemental Information includes four figures and two tables and can be found with this article online at <https://doi.org/10.1016/j.devcel.2018.01.006>.

ACKNOWLEDGMENTS

We thank the UCSD Genomics Core and K. Jepsen for RNA sequencing. We also thank B. Lake and K. Zhang for advice with single-cell sequencing analysis. We thank M. Richardson and Y. Liu for excellent technical assistance, K. Walters for sharing her expertise in follicle counting, S. Chavez for sharing her expertise in single-cell immunofluorescence, M. Belli for sharing her expertise in oocyte chromatin staining and interpretation, and C. Williams for critical reading of the manuscript. H.C.-A. was supported by the Burroughs Wellcome Fund Career Award for Medical Scientists 1015559, Women's Reproductive Health Research grant K12 HD001259, Jones Foundation for Reproductive Medicine, and the American Society for Reproductive Medicine. This research was also supported in part by the Intramural Research Program of the NIH, National Institute of Environmental Health Sciences to P.J.B.

AUTHOR CONTRIBUTIONS

Conceptualization, H.C.-A., J.N.D., K.C., and J.L.-A.; Investigation, H.C.-A., J.N.D., M.R., K.C., D.S., J.L.-A., and S.M.-C.; Resources, D.J.S. and P.J.B.; Writing – Original Draft, H.C.-A., J.N.D., M.R., and J.L.-A.; Writing – Review & Editing, H.C.-A., J.L.-A., M.F.W., J.N.D., K.C., D.S., M.R., L.C.L., S.M.-C., D.J.S., and P.J.B.; Supervision, H.C.-A., M.F.W., and L.C.L.; Funding Acquisition, H.C.-A.

DECLARATION OF INTERESTS

The authors declare no competing interests.

Received: June 26, 2016

Revised: June 21, 2017

Accepted: January 5, 2018

Published: February 5, 2018

REFERENCES

- Andreu-Vieyra, C.V., Chen, R., Agno, J.E., Glaser, S., Anastassiadis, K., Stewart, A.F., and Matzuk, M.M. (2010). MLL2 is required in oocytes for bulk histone 3 lysine 4 trimethylation and transcriptional silencing. *PLoS Biol.* *8*, e1000453.
- Ashburner, M., Ball, C.A., Blake, J.A., Botstein, D., Butler, H., Cherry, J.M., Davis, A.P., Dolinski, K., Dwight, S.S., Eppig, J.T., et al. (2000). Gene ontology: tool for the unification of biology. *The Gene Ontology Consortium. Nat. Genet.* *25*, 25–29.
- Baker, S.C., Bauer, S.R., Beyer, R.P., Brenton, J.D., Bromley, B., Burrill, J., Causton, H., Conley, M.P., Elespuru, R., Fero, M., et al. (2005). The external RNA controls Consortium: a progress report. *Nat. Methods* *2*, 731–734.
- Ball, C.B., Rodriguez, K.F., Stumpo, D.J., Ribeiro-Neto, F., Korach, K.S., Blackshear, P.J., Birnbaumer, L., and Ramos, S.B. (2014). The RNA-binding protein, ZFP36L2, influences ovulation and oocyte maturation. *PLoS One* *9*, e97324.
- Bannister, A.J., and Kouzarides, T. (2011). Regulation of chromatin by histone modifications. *Cell Res.* *21*, 381–395.
- Bouniol-Baly, C., Hamraoui, L., Guibert, J., Beaujean, N., Szöllösi, M.S., and Debey, P. (1999). Differential transcriptional activity associated with chromatin configuration in fully grown mouse germinal vesicle oocytes. *Biol. Reprod.* *60*, 580–587.

- Brooks, S.A., and Blackshear, P.J. (2013). Tristetraprolin (TTP): interactions with mRNA and proteins, and current thoughts on mechanisms of action. *Biochim. Biophys. Acta* 1829, 666–679.
- Brower, P.T., Gizang, E., Boreen, S.M., and Schultz, R.M. (1981). Biochemical studies of mammalian oogenesis: synthesis and stability of various classes of RNA during growth of the mouse oocyte in vitro. *Dev. Biol.* 86, 373–383.
- Burgess, A., Vigneron, S., Brioudes, E., Labbé, J.-C., Lorca, T., and Castro, A. (2010). Loss of human Greatwall results in G2 arrest and multiple mitotic defects due to deregulation of the cyclin B-Cdc2/PP2A balance. *Proc. Natl. Acad. Sci. USA* 107, 12564–12569.
- Burns, K.H., Viveiros, M.M., Ren, Y., Wang, P., DeMayo, F.J., Frail, D.E., Eppig, J.J., and Matzuk, M.M. (2003). Roles of NPM2 in chromatin and nucleolar organization in oocytes and embryos. *Science* 300, 633–636.
- Dahl, J.A., Jung, I., Aanes, H., Greggains, G.D., Manaf, A., Lerdrup, M., Li, G., Kuan, S., Li, B., Lee, A.Y., et al. (2016). Broad histone H3K4me3 domains in mouse oocytes modulate maternal-to-zygotic transition. *Nature* 537, 548–552.
- De La Fuente, R. (2006). Chromatin modifications in the germinal vesicle (GV) of mammalian oocytes. *Dev. Biol.* 292, 1–12.
- de Vries, W.N., Binns, L.T., Fancher, K.S., Dean, J., Moore, R., Kemler, R., and Knowles, B.B. (2000). Expression of Cre recombinase in mouse oocytes: a means to study maternal effect genes. *Genesis* 26, 110–112.
- Dobin, A., Davis, C.A., Schlesinger, F., Drenkow, J., Zaleski, C., Jha, S., Batut, P., Chaisson, M., and Gingeras, T.R. (2013). STAR: ultrafast universal RNA-seq aligner. *Bioinformatics* 29, 15–21.
- Dobin, A., and Gingeras, T.R. (2015). Mapping RNA-seq reads with STAR. *Curr. Protoc. Bioinformatics* 57, 11.14.1-11.14.19.
- External RNA Controls Consortium (2005). Proposed methods for testing and selecting the ERCC external RNA controls. *BMC Genomics* 6, 150.
- Flaws, J.A., Abbud, R., Mann, R.J., Nilson, J.H., and Hirshfield, A.N. (1997). Chronically elevated luteinizing hormone depletes primordial follicles in the mouse ovary. *Biol. Reprod.* 57, 1233–1237.
- Huang, D.W., Sherman, B.T., and Lempicki, R.A. (2009). Systematic and integrative analysis of large gene lists using DAVID bioinformatics resources. *Nat. Protoc.* 4, 44–57.
- Jing, Q., Huang, S., Guth, S., Zarubin, T., Motoyama, A., Chen, J., Di Padova, F., Lin, S.-C., Gram, H., and Han, J. (2005). Involvement of microRNA in AU-rich element-mediated mRNA instability. *Cell* 120, 623–634.
- Kageyama, S., Liu, H., Kaneko, N., Ooga, M., Nagata, M., and Aoki, F. (2007). Alterations in epigenetic modifications during oocyte growth in mice. *Reproduction* 133, 85–94.
- Kharchenko, P.V., Silberstein, L., and Scadden, D.T. (2014). Bayesian approach to single-cell differential expression analysis. *Nat. Methods* 11, 740–742.
- Khare, S.P., Habib, F., Sharma, R., Gadewal, N., Gupta, S., and Galande, S. (2012). Histome – a relational knowledgebase of human histone proteins and histone modifying enzymes. *Nucleic Acids Res.* 40, D337–D342.
- Li, H., Handsaker, B., Wysoker, A., Fennell, T., Ruan, J., Homer, N., Marth, G., Abecasis, G., and Durbin, R.; 1000 Genome Project Data Processing Subgroup (2009). The Sequence Alignment/Map format and SAMtools. *Bioinformatics* 25, 2078–2079.
- Li, L., Zheng, P., and Dean, J. (2010). Maternal control of early mouse development. *Development* 137, 859–870.
- Liu, H., and Aoki, F. (2002). Transcriptional activity associated with meiotic competence in fully grown mouse GV oocytes. *Zygote* 10, 327–332.
- Liu, Y.-J., Nakamura, T., and Nakano, T. (2012). Essential role of DPPA3 for chromatin condensation in mouse ocytogenesis. *Biol. Reprod.* 86, 40.
- Lowther, K.M., and Mehlmann, L.M. (2015). Embryonic poly(A)-binding protein is required during early stages of mouse oocyte development for chromatin organization, transcriptional silencing, and meiotic competence. *Biol. Reprod.* 93, 43.
- Martin, M. (2011). Cutadapt removes adapter sequences from high-throughput sequencing reads. *EMBnet. J.* 17, 10.
- Medvedev, S., Pan, H., and Schultz, R.M. (2011). Absence of MSY2 in mouse oocytes perturbs oocyte growth and maturation, RNA stability, and the transcriptome. *Biol. Reprod.* 85, 575–583.
- Mora-Castilla, S., To, C., Vaezeslami, S., Morey, R., Srinivasan, S., Dumdie, J.N., Cook-Andersen, H., Jenkins, J., and Laurent, L.C. (2016). Miniaturization technologies for efficient single-cell library preparation for next-generation sequencing. *J. Lab. Autom.* 21, 557–567.
- Nagaraj, N., Wisniewski, J.R., Geiger, T., Cox, J., Kircher, M., Kelso, J., Pääbo, S., and Mann, M. (2011). Deep proteome and transcriptome mapping of a human cancer cell line. *Mol. Syst. Biol.* 7, 548.
- Paulo, J.A., and Gygi, S.P. (2017). Nicotine-induced protein expression profiling reveals mutually altered proteins across four human cell lines. *Proteomics* 17, 1600319.
- Ramos, S.B. (2012). Characterization of DeltaN-Zfp36l2 mutant associated with arrest of early embryonic development and female infertility. *J. Biol. Chem.* 287, 13116–13127.
- Ramos, S.B., Stumpo, D.J., Kennington, E.A., Phillips, R.S., Bock, C.B., Ribeiro-Neto, F., and Blackshear, P.J. (2004). The CCCH tandem zinc-finger protein Zfp36l2 is crucial for female fertility and early embryonic development. *Development* 131, 4883–4893.
- Ramsköld, D., Wang, E.T., Burge, C.B., and Sandberg, R. (2009). An abundance of ubiquitously expressed genes revealed by tissue transcriptome sequence data. *PLoS Comput. Biol.* 5, e1000598.
- Sanduja, S., Blanco, F.F., and Dixon, D.A. (2011). The roles of TTP and BRF proteins in regulated mRNA decay. *Wiley Interdiscip. Rev. RNA* 2, 42–57.
- Spasic, M., Friedel, C.C., Schott, J., Kreth, J., Leppke, K., Hofmann, S., Ozgur, S., and Stoecklin, G. (2012). Genome-wide assessment of AU-rich elements by the AREScore algorithm. *PLoS Genet.* 8, e1002433.
- Stumpo, D.J., Broxmeyer, H.E., Ward, T., Cooper, S., Hangoc, G., Chung, Y.J., Shelley, W.C., Richfield, E.K., Ray, M.K., Yoder, M.C., et al. (2009). Targeted disruption of Zfp36l2, encoding a CCCH tandem zinc finger RNA-binding protein, results in defective hematopoiesis. *Blood* 114, 2401–2410.
- Svoboda, P., Franke, V., and Schultz, R.M. (2015). Sculpting the transcriptome during the oocyte-to-embryo transition in mouse. *Curr. Top. Dev. Biol.* 113, 305–349.
- Xia, M., He, H., Wang, Y., Liu, M., Zhou, T., Lin, M., Zhou, Z., Huo, R., Zhou, Q., and Sha, J. (2012). PCBP1 is required for maintenance of the transcriptionally silent state in fully grown mouse oocytes. *Cell Cycle* 11, 2833–2842.
- Zhang, B., Zheng, H., Huang, B., Li, W., Xiang, Y., Peng, X., Ming, J., Wu, X., Zhang, Y., Xu, Q., et al. (2016). Allelic reprogramming of the histone modification H3K4me3 in early mammalian development. *Nature* 537, 553–557.
- Zhang, L., Prak, L., Rayon-Estrada, V., Thiru, P., Flygare, J., Lim, B., and Lodish, H.F. (2013). ZFP36L2 is required for self-renewal of early burst-forming unit erythroid progenitors. *Nature* 499, 92–96.
- Zuccotti, M., Bellone, M., Longo, F., Redi, C.A., and Garagna, S. (2011). Fully-mature antral mouse oocytes are transcriptionally silent but their heterochromatin maintains a transcriptional permissive histone acetylation profile. *J. Assist. Reprod. Genet.* 28, 1193–1196.
- Zuccotti, M., Ponce, R.H., Boiani, M., Guizzardi, S., Govoni, P., Scandroglio, R., Garagna, S., and Redi, C.A. (2002). The analysis of chromatin organisation allows selection of mouse antral oocytes competent for development to blastocyst. *Zygote* 10, 73–78.

STAR★METHODS

KEY RESOURCES TABLE

REAGENT or RESOURCE	SOURCE	IDENTIFIER
Antibodies		
anti-ZFP36L2 (1:2000 for WB)	Sigma	HPA047428; RRID: AB_10963428
anti-ZFP36L2 antibody (for RNA IP)	Abcam	ab70775; RRID: AB_1271231
anti-ZFP36L2 and ZFP36L1 (1:5000 for WB)	Cell Signaling Technologies	2119; RRID: AB_659988
anti-b-Actin (1:5000 for WB)	Sigma	A5316; RRID: AB_476743
anti-H3K4me3 (1:2000 for WB; 1:200 for IF)	Abcam	ab8580; RRID: AB_306649
anti-Histone H3 (1:2500 for WB)	Millipore	05-928; RRID: AB_492621
anti-trimethyl-histone H3 (Lys9) (1:50 for IF)	Millipore	07-442; RRID: AB_310620
pan-histone H3 monoclonal antibody (1:250 for IF)	ThermoFisher Scientific	AHO1432; RRID: AB_1500211
Alexa Fluor 555 conjugated donkey anti-rabbit IgG (H+L) secondary antibody	ThermoFisher Scientific	A-31572; RRID: AB_162543
Alexa Fluor 488 conjugated donkey anti-mouse IgG (H+L) Highly Cross-Adsorbed secondary antibody	ThermoFisher Scientific	A-21202; RRID: AB_141607
Vectashield antifade mounting medium with DAPI	Vector Laboratories	H-1200; RRID: AB_2336790
Chemicals, Peptides, and Recombinant Proteins		
eCG (equine chorionic gonadotropin)	A.F. Parlow, National Hormone and Pituitary Program, National Institute of Diabetes and Digestive and Kidney Diseases, USA (http://www.humc.edu/hormones/material.html)	eCG
hCG	A.F. Parlow, National Hormone and Pituitary Program, National Institute of Diabetes and Digestive and Kidney Diseases, USA (http://www.humc.edu/hormones/material.html)	hCG
Milrinone	Sigma	M4659
Hyaluronidase	Sigma	H4272
Acid Tyrode's Solution	Millipore	MR-004-D
2x Laemmli sample buffer	Bio-Rad	1610737
Detector™ Block buffer	KPL	71-83-00
SuperSignal™ West Dura Extended Duration Substrate	ThermoFisher scientific	34075
Trizol	ThermoFisher scientific	15596
Actinomycin D	Sigma	A9415
Critical Commercial Assays		
SMARTer® Ultra® Low Input RNA Kit for Sequencing - v3	Clontech	634851
Nextera XT DNA library preparation kit	Illumina	FC-131-1024
Power SYBR Green Cells-to-Ct kit	Life Technologies	4402953
Click-iT RNA Alexa Fluor 488 Imaging kit	Invitrogen	C10329, C10330
Magna RIP RNA-binding protein Immunoprecipitation Kit	EMD Millipore	17-700
TURBO DNA-free kit	ThermoFisher scientific	AM1907

(Continued on next page)

Continued		
REAGENT or RESOURCE	SOURCE	IDENTIFIER
Silentfect Lipid Reagent for RNAi	Bio Rad	1703361
Deposited Data		
Raw and analyzed data	This paper	GEO: GSE96638
Experimental Models: Cell Lines		
HeLa	ATCC	HeLa (ATCC® CRM-CCL-2™)
Experimental Models: Organisms/Strains		
Conditional <i>Zfp36l2</i> knockout mouse (C57BL/6 Background)	Xenogen Biosciences; D.J. Stumpo and P.J. Blackshear, unpublished data	Not yet commercially available
Oligonucleotides		
siRNA against <i>Zfp36l2</i> (guuguggaugaaguggcagcg)	(Jing et al., 2005)	(siZFP36)
siRNA against Luciferase (cguacgcggaauacuucga)	(Jing et al., 2005)	(siCtrl)
See Table S2 for a list of primers	N/A	N/A
Software and Algorithms		
cutadapt (v1.8.1)	(Martin, 2011)	DOI: https://doi.org/10.14806/ej.17.1.200
STAR (2.3.0.1)	(Dobin et al., 2013; Dobin and Gingeras, 2015)	https://github.com/alexdobin/STAR
scde (v.1.2.1)	(Kharchenko et al., 2014)	http://hms-dbmi.github.io/scde/
Samtools	(Li et al., 2009)	http://samtools.sourceforge.net/
rpkmforgenes.py	(Ramsköld et al., 2009)	http://sandberg.cmb.ki.se/media/data/maseq/instructions-rpkmforgenes.html
AmiGO	(Ashburner et al., 2000)	http://amigo.geneontology.org/amigo
Histome	(Khare et al., 2012)	http://www.actrec.gov.in/histome/
DAVID Bioinformatics Resources 6.8	(Huang et al., 2009)	https://david.ncifcrf.gov/
AREScore	(Spasic et al., 2012)	http://arescore.dkfz.de/arescore.pl
Other		
M2 Media	Sigma	M7167
M16 Media	Sigma	M7292
ERCC Spike-In RNAs	Life Technologies (1:25,000 dilution)	4456740
Superscript IV reverse transcriptase	ThermoFisher scientific	18090050
SsoAdvanced Universal SyBr Green Supermix	Bio-Rad	1725274
Immobilon-P membranes	Millipore	IPVH00010
iScript Reverse transcription supermix	Bio-rad	1708840
DMEM Media	Gibco	11995073
Fetal Bovine Serum, Heat Inactivated	Hyclone	SH30071.03HI
Penicillin/Streptomycin	Gibco	15140-122
0.25% Trypsin-EDTA	Gibco	25200-114

CONTACT FOR REAGENT AND RESOURCE SHARING

Further information and requests for resources and reagents should be directed to and will be fulfilled by the Lead Contact, Heidi Cook-Andersen (hcookandersen@ucsd.edu).

EXPERIMENTAL MODEL AND SUBJECT DETAILS

Generation of Conditional Knockout Mice

Conditional *Zfp36l2* knockout mice were generated by Xenogen Biosciences (Cranbury, NJ) using standard embryonic stem (ES) cell targeting techniques. These mice will be described in detail in a future study (D.J. Stumpo and P.J. Blakeshear, unpublished data). The targeting construct was designed to delete exon 2, which contains the RNA binding domain and the majority of the protein coding region. Briefly, C57BL/6 genomic DNA was used to prepare a targeting vector that contained loxP sites flanking exon 2 as well as a Neomycin (Neo) positive selection expression cassette. C57BL/6 ES cells were electroporated with the targeting vector and correctly targeted ES cells were subsequently transiently transfected with a Flp expressing plasmid to excise the Neo cassette. Blastocysts were injected with two independent clones and germline transmission was obtained by crossing chimeras with C57BL/6 Tac wild type mice. Heterozygous mice with a conditional floxed *Zfp36l2* allele were intercrossed to generate homozygous floxed mice. Deletion of *Zfp36l2* by conditional knock out was obtained by crossing the oocyte-specific *Zp3-Cre* transgenic mice with the *Zfp36l2* floxed mice (*Zfp36l2^{fl/fl}*) to generate *Zfp36l2^{fl/fl};Zp3-Cre* males that were then mated with *Zfp36l2^{fl/fl}* females to generate *Zfp36l2-cKO* and *-Fl/Fl* littermate controls for experiments. For each experiment detailed below, the total number and age of mice used are clearly stated. Mice were genotyped by polymerase chain reaction (primers used for genotyping are provided in [Supplemental Information](#)). The C57BL/6 mice colonies were maintained in agreement with protocols approved by the Institutional Animal Care and Use Committee at the University of California, San Diego.

Primary Culture of Oocytes and Zygotes

For experiments involving primary culture of oocytes, female mice at the ages specified in the description of each experiment, were stimulated with intraperitoneal injection 10 IU equine Chorionic Gonadotropin (eCG; A.F. Parlow, National Hormone and Pituitary Program, National Institute of Diabetes and Digestive and Kidney Diseases, USA), ovaries were harvested 44 hours after eCG injection, and GV oocytes were collected following ovarian puncture in M2 media (Sigma) containing 5 μ M Milrinone. For *in vitro* oocyte maturation assessment, oocytes were washed 5 times to remove the Milrinone (Sigma) and intact COC complexes were cultured for 18-20 hours at 37°C in M2 media. To obtain zygotes, 5 to 8-wk-old female mice were superovulated with intraperitoneal injection 10 IU eCG followed by 10 IU of human Chorionic Gonadotropin (hCG; A.F. Parlow, National Hormone and Pituitary Program, National Institute of Diabetes and Digestive and Kidney Diseases, USA) 46 hours later. The female mice were placed with 8-12-wk-old WT males of known fertility at the time of hCG injection. The contents of the ampulla were collected only from females with a visible plug 18 hrs after hCG injection. Ampulla contents were evaluated for the presence of zygotes by microscopy following a brief digestion in hyaluronidase (Sigma). Isolated cells were cultured overnight in M16 media (Sigma) to confirm fertilization and/or fertilization failure.

Maintenance of Cell Lines

HeLa cells (ATCC) were grown in DMEM (Gibco) supplemented with 10% FBS (Hyclone) and 1% Penicillin/Streptomycin (Gibco), and were split using 0.25% Trypsin-EDTA (Gibco) approximately every two days, when cells reached 80% confluence. Experiments were performed on cells once they reached approximately 80% confluence.

METHOD DETAILS

Genotyping and DNA PCR

Ear tags were taken from mice and DNA was extracted for PCR (Viagen, Cat# 102-T). Lysed ear tags were heated at 55°C for 3-4 hours and then 85°C for 1 hour to denature lysozymes in the buffer. PCR reactions were conducted in 25 μ L volume reactions with 1 μ L lysed mouse DNA, 19.5 μ L nuclease free water, 1 μ L dNTP mixture (BioPioneer, Cat# MDM-4), 0.5 μ L forward and reverse primer mixture (10 μ M), 2.5 μ L 10x buffer (Denville, cat# CB3702-7), and 0.5 μ L Taq polymerase (Denville, Cat# CB4050-2). 1.2% agarose gel with ethidium bromide was used for visualization of gene bands. Primers used are listed in [Table S2](#).

Fertility and Estrus Cycle Assessment

Zfp36l2-Fl/Fl (n=7), *Zfp36l2-cKO* (n=8), and WT (n=8) females were individually set up in breeding pairs with WT males of known fertility and followed for 6 months. At the time breeder cages were set up, female mice were between 8-16 weeks old. Males in each breeding pair were exchanged at 6 months of age. Maternal abdomens were monitored for swelling suggestive of pregnancy. Cages were checked daily to ensure that newly born pups were counted before potential cannibalization. To evaluate mating behavior, 6 WT male (aged 7-8 weeks) and *Zfp36l2-cKO* virgin female (aged 9-10 weeks) pairs were set up and females were evaluated each morning for 44 consecutive days for the presence or absence of a seminal vaginal plug. To assess estrus cycle length, *Zfp36l2-cKO* and *Zfp36l2-Fl/Fl* female mice (n = 3 at 15-19 weeks old for each genotype) were housed in individual cages for 25 days to obtain at least three full estrus cycles from each mouse. Females were housed individually for at least 1 month prior to the start of the experiment. Each day, a sterile pipette and 50 μ L of water were used to obtain a vaginal smear from each mouse. Vaginal smear slides were stained with 0.4% methyl blue and analyzed to determine the estrus cycle stage for each mouse each day using standard published criteria. Estrus length was defined as the time between two consecutive estrus observations.

Ovarian Follicle Counts

Unstimulated ovaries were collected from singly-housed, unstimulated adult cKO and Fl/Fl females aged 15–23 weeks of age in the diestrus phase of the cycle ($n = 7$ for each genotype). Stimulated ovaries were isolated from sexually immature, 4–5 week old females 46 hours following intraperitoneal injection 10 IU eCG ($n = 3$ for each genotype). Whole ovaries from cKO and *Zfp36l2*-Fl/Fl mice were fixed in neutral buffered formalin for 16–24 hours. Whole ovaries were processed in pairs, embedded in paraffin wax and then cut in 5 μm sections. All slides were Haematoxylin and Eosin stained using standard protocols and scanned using Zeiss Axio Scan.Z1. Every fifth section, of one ovary per mouse, was analyzed with respect to the number and stage of follicles. Follicles were only counted if nucleus was clearly visible to avoid duplicate counting. Counts were binned into the following stage categories: Primordial (Pr), Primary (1^0), Secondary (2^0), Antral (Ant), Corpus luteum (CL), Atretic (Atr). To correct for counting only every fifth section, total ovary counts were multiplied by five as per published protocols (Flaws et al., 1997). Statistical analysis was performed using GraphPad Prism. All p-values obtained through unpaired T-tests.

Evaluation of Oocyte Diameter

To measure oocyte diameter, 5 week-old *Zfp36l2*-Fl/Fl and -cKO female mice (4 mice per genotype) were stimulated with intraperitoneal injection 10 IU eCG, ovaries were harvested 44 hours after eCG injection, and GV oocytes were collected following ovarian puncture in M2 media (Sigma) containing 5 μM Milrinone (Sigma). All GV oocytes completely enclosed in cumulus cells were collected, stripped of granulosa cells mechanically with pipetting, and photographed. Oocyte diameters were determined by measurement of the images using NIH Image J software and a scale for calibration, measuring both the largest diameter the diameter perpendicular to this line, both exclusive of the zona pellucida. The oocyte diameters and distribution for each group were determined using Prism (GraphPad Software).

Ovulation, Maturation and Fertilization

To evaluate maturation and ovulation rates *in vivo*, 5 to 8 week-old female mice were superovulated with intraperitoneal injection 10 IU eCG followed by 10 IU of hCG 46 hours later to trigger oocyte maturation and ovulation. Oocytes released from the ovary were collected from the ampulla 15 hrs after hCG injection and cumulus cells were removed by brief hyaluronidase digestion per standard protocol and evaluated under the dissection microscope (Leica M125). The data presented is from oocytes pooled from 9 mice of each genotype in 3 separate experiments. To evaluate maturation rates *in vitro*, 5 to 8 wk-old female mice were stimulated with 10 IU of eCG by intraperitoneal injection. To isolate periovulatory, germinal vesicle (GV) stage oocytes, the mice were sacrificed 46 hrs after eCG injection, the ovaries were harvested and follicles were collected following ovarian puncture in M2 media containing 5 μM Milrinone. Only oocytes completely enclosed in cumulus cells were collected. Oocytes were washed 5 times to remove the Milrinone and intact COC complexes were cultured for 20 hours at 37°C in M2 media before assessment for polar body extrusion by microscopy. A total of 102 Fl/Fl and 57 cKO oocytes were assessed from 5 mice of each genotype in 2 separate experiments. To test fertilization and obtain zygotes, 5 to 8-wk-old female mice were superovulated with intraperitoneal injection 10 IU eCG followed by 10 IU of hCG 46 hours later. The female mice were placed with 12-wk-old WT males of known fertility at the time of hCG injection. The next morning, the female mice were checked for vaginal plug. The contents of the ampulla were collected only from females with a visible plug 18 hrs after hCG injection. Ampulla contents were evaluated for the presence of zygotes by microscopy following a brief digestion in hyaluronidase (Sigma). Isolated cells were cultured overnight to confirm fertilization and/or fertilization failure. A total of 95 zygotes from 5 *Zfp36l2*-Fl/Fl females were evaluated.

Single Cell Library Preparation

Five week-old *Zfp36l2*-Fl/Fl and -cKO female mice were stimulated with 10 IU of eCG by intraperitoneal injection. The mice were sacrificed 46 hrs after eCG injection, ovaries were harvested and GV oocytes were collected following ovarian puncture in M2 media containing 5 μM Milrinone. Only oocytes completely enclosed in cumulus cells were collected and granulosa cells were mechanically removed using pipets of decreasing diameter. The zona pellucida was removed with a brief incubation in Acid Tyrode's solution (Millipore) and the oocytes were immediately washed in PBS with 0.1% BSA. Single mouse oocytes were transferred into nuclease free 0.2ml PCR tubes and placed immediately on dry ice. In total, 26 Fl/Fl oocytes and 24 cKO oocytes were analyzed from 4 separate littermate pairs for each genotype in 4 separate experiments. As an additional means of normalization, ERCC Spike-In RNAs (Life Technologies, Cat.no. 4456740) were added to the first set of samples, which comprised 9 Fl/Fl and 7 cKO single oocytes. The ERCC stock provided by the manufacturer was diluted 1:25,000 and 0.25 μl of the dilution was added to each oocyte before cell lysis and RNA-seq library preparation, and ERCC reads were analyzed downstream in parallel with reads from the oocyte transcriptome. RNA isolation and cDNA synthesis was carried out using the SMARTer® Ultra® Low Input RNA Kit for Sequencing - v3 (Clontech, Cat.no. 634851). Libraries were generated from the resulting cDNA using the Nextera XT DNA library preparation kit (Illumina, Cat.no. FC-131-1024) as previously described (Mora-Castilla et al., 2016).

RNA Sequencing and Data Analysis

Approximately 21.5 million reads were generated per sample, and 58% of these reads were uniquely mapped via STAR (v2.3.0.1) (Dobin et al., 2013) after trimming for low quality reads and adapter sequences via cutadapt (v1.8.1) (Martin, 2011). Processing of .sam files was accomplished with Samtools (Li et al., 2009). Counts for each gene were quantified using the python script rpkmfor-genes.py (Ramsköld et al., 2009) and annotated using the Refseq mm10 genome, which had been concatenated with the ERCC

Spike-In annotation. Reads were filtered, such that genes without at least one sample with at least 10 raw reads and one RPKM read were removed from the analysis, and overlapping RefSeq transcripts were collapsed giving one expression value per gene locus. The count data was normalized and differential expression was performed using the R (v.3.1.1) package *scde* (v.1.2.1). Briefly, *scde* accounts for technical noise by fitting individual error models for single cell RNA-seq measurements. This Bayesian approach estimates both the likelihood of a gene being expressed in a given cell as well as expression fold change between subpopulations (Kharchenko et al., 2014). Genes with an adjusted P value (Q-value) less than 0.05 were considered differentially expressed unless otherwise noted. Heatmaps, scatter plots, and boxplots were constructed using the R (v.3.1.1) package *gplots*. GO categories for heatmaps were compiled with *AmiGO* (v2.3.2) (Ashburner et al., 2000) and *HlStome* (Khare et al., 2012). All functional enrichment analyses were generated using DAVID gene annotation and analysis resource (Huang et al., 2009). AU-rich elements were quantified using the *AREScore* algorithm (Spasic et al., 2012). Cumulative plots in Figures S2 and S3 were generated from custom Python scripts using ZFP36L2 RIP data from Zhang et al. (Zhang et al., 2013), *AREScores* from Spasic et al. (Spasic et al., 2012), GO terms from *AmiGO* (Ashburner et al., 2000), and single cell RNA seq data from this study with Upregulated and Downregulated transcripts defined as described above (Q<0.05), and log₂ fold change (cKO/WT) values calculated for transcripts using the *scde* algorithm (Kharchenko et al., 2014).

RNA Isolation and qPCR Analysis

GV oocytes were isolated from FI/FI and cKO females aged 5 to 8 weeks in M2 media supplemented with 5 μM Milrinone following eCG stimulation, ovarian follicle puncture and mechanical removal of granulosa cells as described above. One hundred mouse oocytes of each genotype were isolated and pooled from 3-10 mice of each genotype in at least 3 separate experiments using quantitative real time PCR (qPCR). *Gapdh* or *L19* were used as an endogenous controls. RNA isolation, cDNA synthesis and qPCR reactions were set up according to the instructions in the Power SYBR Green Cells-to-Ct kit (Life Technologies, Cat. no. 4402953) per the manufacturer's protocol with the exception that lysis of the 100 oocyte samples was performed in 50 microliters of lysis buffer. The cDNA generated was used for gene expression analysis in triplicate by qPCR with custom synthesized primers and details of the primers used are listed in Table S2. qPCR was performed in at least 2 pools of oocytes from at least 10 mice of each genotype.

Run-on Transcription Assays

GV oocytes were isolated from FI/FI and cKO females aged 5 to 8 weeks in M2 media supplemented with 5 μM Milrinone following eCG stimulation, ovarian follicle puncture and mechanical removal of granulosa cells as described above. Mice were age-matched for each experiment and littermate controls were used when possible. The last 5 washes were carried out in M2 medium alone to remove the milrinone. Transcriptional activity was determined in run-on studies with 5-ethynyl-uridine (EU) using the Click-iT RNA Alexa Fluor 488 Imaging kit (Invitrogen, C10329, C10330). The oocytes were cultured in M2 medium with or without 2mM EU at 37°C for 45 minutes. After the incubation in EU, the oocytes were then transferred to Acid Tyrode's solution briefly to remove the zona and washed three times in Phosphate Buffered Saline (PBS) with Bovine Serum Albumin (BSA). The oocytes were then immediately fixed in 4% Paraformaldehyde (PFA) for 30 minutes and washed three times in PBST as above. The oocytes were then permeabilized in 0.1% Triton X-100 in PBS 1 hour at room temperature and washed 3 times in PBST. The oocytes were then incubated for 30 minutes at room temperature with the Click-iT reaction cocktail prepared per the manufacturer's protocol and washed again 3 times with PBST. DNA staining was performed using Hoechst 33342 at 1:1000 in PBST for 15 minutes immediately prior to imaging. SN was assigned to nuclei demonstrating a complete ring of chromatin around the nucleolus when visualized by confocal microscopy at 40X magnification. The fluorescent signal was detected using the 40X objective of a laser-scanning confocal microscope (Zeiss LSM780). As above, to accurately compare fluorescent intensity between oocytes, the laser power was set based upon the oocyte with the strongest signal and the same setting was used to evaluate all oocytes. A total of 140 and 80 oocytes were screened from 7 *Zfp36l2*-FI/FI and 10 *Zfp36l2*-cKO mice, respectively, in 2 separate experiments.

Western Blotting

GV oocytes were isolated from FI/FI and cKO females aged 5 to 8 weeks in M2 media supplemented with 5 μM Milrinone following eCG stimulation, ovarian follicle puncture and mechanical removal of granulosa cells as described above. An equal number of FI/FI and cKO GV oocytes were lysed in 25 ml of RIPA lysis buffer, incubated on ice for 1 hour and then mixed with the same volume of 2x Laemmli sample buffer (Bio-Rad, Cat. No. 1610737). After boiling for 10 minutes, total lysate was fractionated on SDS-PAGE and Western blotting was performed following transfer to Immobilon-P membranes (Millipore, Cat. No. IPVH00010) using standard protocols. Blocking was performed using Detector™ Block buffer (KPL, Cat. No. 71-83-00) and detection was performed using SuperSignal™ West Dura Extended Duration Substrate (ThermoFisher scientific, Cat. No. 34075). For ZFP36L2, 50 GV oocytes were loaded per lane; for H3K4me3, 70 GV oocytes were loaded per lane. Primary antibodies and dilutions used were as follows: anti-ZFP36L2 (1:2000, Sigma HPA047428); anti-b-Actin (1:5000, Sigma, Cat. No. A5316); anti-H3K4me3 (1:2000, Abcam, Cat. No. ab8580) and anti-Histone H3 (1:2500, Millipore, Cat. No. 05-928). Internal loading controls were detected on the same membrane. Detection of each target was performed at least twice using pooled oocytes from different mice.

Immunofluorescence

GV oocytes were isolated from FI/FI and cKO females aged 5 to 8 weeks in M2 media supplemented with 5 μ M Milrinone following eCG stimulation, ovarian follicle puncture and mechanical removal of granulosa cells as described above. The zona pellucida was removed in Acid Tyrode's solution, followed by three washes in PBS with 0.1% BSA. The oocytes were fixed with 4% PFA in PBS for 1 hour at room temperature followed by three washes in PBS with 0.1% BSA and 0.1% Tween (PBST). The oocytes were then permeabilized by incubation with 1% Triton X-100 in PBS for 15 minutes at room temperature. After permeabilization, the oocytes were again washed three times in PBST and blocked with 4% normal donkey serum in PBST for 1 hr at room temperature. The oocytes were incubated with primary antibodies overnight at 4°C. All washes and incubations were performed with gentle agitation. Anti-histone H3 (tri methyl K4) antibody (Abcam, Cat. No. ab8580) was used at a dilution of 1:200, anti-trimethyl-histone H3 (Lys9) antibody (Millipore, Cat. No. 07-442) was used at a dilution of 1:50, and pan-histone H3 monoclonal antibody (ThermoFisher Scientific, Cat. No. AHO1432) was used at a dilution of 1:250. After removing the primary antibody, the oocytes were washed three times in PBST and then incubated with Alexa Fluor 555 conjugated donkey anti-rabbit IgG (H+L) secondary antibody (ThermoFisher Scientific, Cat. No. A-31572) or Alexa Fluor 488 conjugated donkey anti-mouse IgG (H+L) Highly Cross-Adsorbed secondary antibody (ThermoFisher Scientific, Cat. No. A-21202) for 1 hour at room temperature. The oocytes were then washed three times with PBST and mounted in 96 well glass bottom plates with a 50% dilution of Vectashield antifade mounting medium with DAPI (Vector Laboratories, Cat. No. H-1200). The fluorescent signal was detected using the 40X objective of a laser-scanning confocal microscope (Zeiss LSM780). To accurately compare fluorescent intensity between oocytes, the laser power was set based upon the oocyte with the strongest signal and the same setting was used to evaluate all oocytes. Signal quantification was performed using NIH Image J software; Corrected Total Cell Fluorescence (CTCF) was calculated as $CTCF = \text{Integrated density} - (\text{Area of selected region} \times \text{Mean fluorescence of background readings})$ (Burgess et al., 2010). CTCF was calculated for H3K4me3, H3K9me3, total H3, and DAPI signals; H3K4me3, H3K9me3, and total H3 were normalized to the DAPI signal for each oocyte nucleus. Significance as demonstrated in Figure 5B and the corresponding figure legend was calculated with an unpaired Student's parametric T-test, with error bars representing SEM. Greater than 40 oocytes pooled from 15 mice were examined in 4 separate experiments for each histone target.

RNA Immunoprecipitation

Magna RIP RNA-binding protein Immunoprecipitation Kit (EMD Millipore, Cat. No. 17-700) was used for RIP assay, with some modifications from the manufacturer's protocol. In brief, 80-90% confluent HeLa cells in 6X10 cm plates were dissolved in 300 ml of lysis buffer and supernatants were harvested as cell lysates after centrifugation at 14,000 rpm for 10 minutes. Cell lysates were pre-cleared by incubating with washed magnetic beads for 1 hour at 4°C. During pre-clearing, 5 mg of anti-ZFP36L2 antibody (Abcam, Cat. No. ab70775) was bound to pre-washed magnetic beads by incubating with rotation for 30 minutes at room temperature (RT) and 5 mg of purified rabbit IgG was bound to pre-washed magnetic beads as a negative control. Pre-cleared lysate was divided into two parts and incubated overnight at 4°C with anti-ZFP36L2 antibody-bound magnetic beads or rabbit IgG-bound magnetic beads, respectively. On the following day, beads were washed 6 times with RIP wash buffer and then treated with proteinase K for 30 minutes at 55°C. Supernatants were separated using a magnetic separator, transferred into new tubes, and then cleaned by phenol chloroform extraction. Nucleotides were isolated by ethanol precipitation and re-suspended in 12.5 ml RNase-free water. DNA was removed by using TURBO DNA-free kit (ThermoFisher scientific, Cat. No. AM1907) and then cDNA was synthesized using superscript IV reverse transcriptase (ThermoFisher scientific, Cat. No. 18090050). Quantitative real time PCR assay was performed using SsoAdvanced Universal SyBr Green Supermix (Bio-Rad, Cat. No. 1725274). Primers used in for qPCR are shown in Table S2. Graph in Figure 4B represents average values of 5-6 independent experiments. For normalization, fold enrichment of each RNA in the anti-ZFP36L2 antibody-precipitated sample was determined relative to the rabbit IgG precipitated sample and values were then normalized to the value for L19. Statistical significance was calculated via two-way ANOVA, after log transformation to generate a more normal distribution of the data.

RNA Decay Assays

HeLa cells cultured on 6 well-plates were transfected with either 20mM of siRNA targeting human ZFP36 family members (siZFP36; guuguggaugaaguggcagcg) (Jing et al., 2005) or siRNA against Luciferase (siCtrl: cguacgcggaauacuucga) using Silentfect Lipid Reagent for RNAi (Bio Rad, Cat. No. 1703361). At 24 hours post-transfection, cells were transfected again with the same siRNAs and incubated for another 24 hours. Then, cell culture media was exchanged with fresh media and, at 2 hours after media exchange, cells were treated with 0.5 mg/ml of Actinomycin D (Sigma) for 0 hours, 1 hour, 2 hours and 4 hours. Western blotting was performed as above using an antibody that recognizes both ZFP36L2 and ZFP36L1 (Cell Signaling Technologies Cat. No. 2119) at 1:5000 dilution. ZFP36L1 and ZFP36 were not detectable by Western blotting before or after siRNA treatment (data not shown), consistent with published data (Nagaraj et al., 2011; Paulo and Gygi, 2017). GAPDH served as loading control. Total RNAs were isolated from cells using Trizol reagent (ThermoFisher scientific, Cat. No. 15596) and qRT-PCR was performed using iScript Reverse transcription supermix (Bio-rad, Cat. No. 1708840) and SsoAdvanced Universal SyBr Green Supermix (Bio-Rad, Cat. No. 1725274). Half-lives were calculated by nonlinear regression, with an exponential fit, using GraphPad Prism Software and presented in hours. Data were plotted on a logarithmic y-axis to show a linear best-fit line. Accurate half-lives could not be calculated for mRNAs for which the regression line was near horizontal.

ARE Conservation

3'UTR sequences for indicated transcripts were compiled from the NCBI Gene database. For genes with more than one transcript, that with the highest AREScore (typically the longest transcript) was used for analysis. AREScores were determined with the AREScore algorithm, using the 3'UTR fasta sequences as input (Spasic et al., 2012).

QUANTIFICATION AND STATISTICAL ANALYSIS

Statistical analysis and software used have already been detailed in the methods sections above, associated with each experiment, as well as in the figure legends. To summarize, all statistical comparisons seen in the main and supplementary figures, unless otherwise specifically stated in the detailed experimental methods above, were conducted using an unpaired T-test, where error bars represent standard error of the mean (SEM). In cases where data did not meet the assumptions of the statistical approach (i.e., normal distribution), a logarithmic transformation of the data was first conducted, followed by the statistical test. Statistical analysis associated with cumulative distribution plots was conducted using the nonparametric Kolmogorov-Smirnov (KS) test, which is appropriate for comparing probability distributions. For RNA sequencing analysis, count data was normalized to ERCC spike-in concentration, as well as to the whole genome using Reads Per Kilobase of transcript per Million of mapped reads (RPKM). Differential expression was performed using the R (v.3.1.1) package scde (v.1.2.1), which accounts for technical noise by fitting individual error models for single cell RNA-seq measurements. This Bayesian approach estimates both the likelihood of a gene being expressed in a given cell as well as expression fold change between subpopulations, adding robustness to single-cell differential expression analysis (Kharchenko et al., 2014). Genes with an adjusted P value (Q-value) less than 0.05 were considered differentially expressed unless otherwise noted, taking into account multiple testing in genome-wide comparisons. RNA half-life was calculated by nonlinear regression, using an exponential fit; the data is plotted on a logarithmic y-axis for clarity of presentation. All statistical calculations were conducted using GraphPad Prism Software, R (v.3.1.1), and python.

DATA AND SOFTWARE AVAILABILITY

The RNA sequencing data associated with this study have been made publicly available under the accession number GEO: GSE96638. Additional data tables, including read counts, differential expression quantification, and calculation of transcript-associated AREScores (Spasic et al., 2012) are available in Table S2. Software used for all statistical analysis includes GraphPad Prism, R (v3.1.1), and python. Specific R packages used include scde (v.1.2.1) and gplots. RNA sequencing data was trimmed of poor-quality sequences and adapter content with cutadapt (Martin, 2011), mapped with STAR (Dobin et al., 2013; Dobin and Gingeras, 2015) to the Refseq mm10 genome, and file formats were converted with Samtools (Li et al., 2009). Reads were quantified using the python script rpkmforgenes.py (Ramsköld et al., 2009). Publicly available programs used for various computational analyses include the AREScore algorithm (Spasic et al., 2012), DAVID Gene Ontology Analysis (Huang et al., 2009), AmiGO (Ashburner et al., 2000), and HlStome (Khare et al., 2012). Custom Python scripts for generation of cumulative plots in Figures S2 and S3 are available upon request.